IEEE Access
Multidisciplinary | Rapid Review | Open Access Journal

Received March 5, 2021, accepted March 19, 2021, date of publication March 23, 2021, date of current version April 1, 2021.

Digital Object Identifier 10.1109/ACCESS.2021.3068211

Robust Color Images Watermarking Using New Fractional-Order Exponent Moments

KHALID M. HOSNY[1], (Member, IEEE), MOHAMED M. DARWISH[2], AND MOSTAFA M. FOUDA[3], (Senior Member, IEEE)

[1]Department of Information Technology, Faculty of Computers and Informatics, Zagazig University, Zagazig 44519, Egypt
[2]Department of Computer Science, Faculty of Computers and Information, Assiut University, Assiut 71516, Egypt
[3]Department of Electrical and Computer Engineering, Idaho State University, Pocatello, ID 83209, USA

Corresponding author: Khalid M. Hosny (k_hosny@yahoo.com)

ABSTRACT Robust watermarking is a valuable methodology used in protecting the copyright and securing digital images. In this paper, new fractional-order multi-channel orthogonal exponent moments (MFrEMs) and their invariants to geometric transformations are derived for the first time. We utilized these highly accurate moments to construct a new robust watermarking algorithm for color images. This algorithm consists of three phases. First, the bits of the binary watermark scrambled by using a 1D Sine chaotic map. Second, the fractional-order MFrEMs are calculated from the host color image. Finally, a quantization process is performed, where the scrambled bits of the binary watermark embedded into the host color image. Various experiments were conducted to test the proposed watermarking algorithm and compare it with the existing robust watermarking algorithms for color images. The obtained results ensure the proposed robust watermarking algorithm's superiority over existing algorithms regarding the visual imperceptibility and robustness against various attacks.

INDEX TERMS Robust watermarking, fractional-order orthogonal moments, sine mapping, geometric attacks.

I. INTRODUCTION

With the rapid advancement of color images and the widespread use of sophisticated tools for editing digital content, the door opened for various problems, such as tampering, modification, forgery of digital contents, and infringement of intellectual property rights. Therefore, protecting copyright content and digital images' integrity increases and becomes a significant security matter [1]. Digital watermarking is widely used in the protection of digital content [2]. Methods of watermarking are classified into robust watermarking [3], semi-fragile watermarking [4], and fragile watermarking [5]. Both semi-fragile and fragile watermarking methods are sensitive to partial or complete modification. On the other side, the robust watermarking technique is resisting common attacks. Fazli and Moeini [6] show that when geometric attacks attack watermarked images, translation, scaling, and rotation (TSR), extracting the watermark is challenging. Therefore, robustness and imperceptibility are the most critical performance requirements—a watermarking algorithm's ability to resist attacks is called robustness. Wang *et al.* [7] showed that imperceptibility reflects the cover image's visual quality after attacks.

A successful watermarking algorithm should resist TSR and other attacks such as noise, compression, etc. Alghoniemy *et al.* [8] utilized the geometric moment invariants (Hu moments) for the first time to construct a robust watermarking algorithm. Many geometric invariant watermarking algorithms [9]–[12] proposed various orthogonal moments. However, these watermarking techniques are presented to deal with grey-level images. In recent years, color imaging technologies improved, and color image processing's interest gained more attention, so color image watermarking became an active research topic.

Researchers focus on robust color image watermarking to resist geometric attacks. Tsougenis *et al.* [13] used non-orthogonal quaternion radial moments in color image watermarking. On the other side, researchers utilized orthogonal quaternion moments such as exponent moments (QEMs) [14], radial harmonic Fourier moments (QRHFMs) [15], and polar harmonic transforms (QPHTs) [16] in geometrically invariant watermarking. Wang *et al.* [17] and

The associate editor coordinating the review of this manuscript and approving it for publication was Di He.

Xu *et al.* [18] utilized QEMs and QPHTs in robust color image watermarking. In [13]–[18], the quaternion moments computed using the approximated Zero-order method (ZOA), which results in numerical errors and instability, especially at high moment orders. The utilization of inaccurate quaternion moments led to bad imperceptibility and low robustness, which are challenging problems.

To overcome these challenges, Hosny and Darwish proposed two accurate watermarking methods for color images. The first is the quaternion Legendre-Fourier moments (QLFMs) [19], while the second one is the quaternion radial substituted Chebyshev moments (QRSCMs) [20].

Researchers in their recent works [21]–[24] used different chaotic maps with moment-based watermarking algorithms to increase security. Ma *et al.* [25] combined invariant accurate polar harmonic Fourier moments with chaotic mapping for robust watermarking of grey-level images. These moment-based methods for image watermarking are limited to utilizing orthogonal moments of integer-orders. Recent studies [26]–[31] proved that polynomials with fractional orders have a better ability to represent functions than their corresponding integer orders. Yamni *et al.* [32], [33] used fractional-order Charlier moments to reconstruct and watermarking grey-level images. Chen *et al.* [34] utilized quaternion discrete fractional random transform for adaptive watermarking of color images.

Recent fractional-order moments' intrinsic characteristics motivate the authors to propose novel fractional-order exponent moments with their invariants to the geometric transformations. Then the authors utilized these invariant geometric moments with a Sine mapping to construct a highly accurate and robust reversible watermarking for color images.

In this work, a new watermarking algorithm with high resistance ability to various attacks is proposed. This algorithm utilized new fractional-order multi-channel orthogonal exponent moments (MFrEM) and Sine mapping. In this algorithm, orthogonal exponent Fourier functions of fractional orders are derived. These functions are used to formulate new fractional-order multi-channel orthogonal exponent moments (MFrEM). The rotation, scaling, and translation (RST) invariants of these fractional-order moments are derived. We used a highly accurate computation method to compute MFrEM based on Gaussian numerical integration for radial kernels and exact integration for angular kernels, which significantly improved the accuracy of MFrEM. Finally, a one-dimensional (1D)-chaotic Sine map is utilized to enhance security.

Chaotic mapping is used because of its superiority in terms of ergodic uniformity and the ability to increase the algorithm's speed in finding the optima while generating initial values uniformly distributed within the range of [0, 1]. The performance of the algorithm and the comparison with existing methods are evaluated through a series of experiments. The proposed watermarking algorithm outperformed existing methods.

The remainder of this paper is organized as follows. Section II presents the proposed fractional-order multi-channel orthogonal exponent moments and their geometric invariances. A detailed description of the proposed watermarking algorithm is proposed in Section III. Section IV presents a description of the performed experiments. Section V concludes the paper.

II. FRACTIONAL-ORDER ORTHOGONAL MOMENTS

A. THE DEFINITION OF MFrEMs FOR RGB COLOR IMAGES

Exponent moments are circular orthogonal moments [35]:

$$M_{pq} = \frac{1}{4\pi}\int_0^{2\pi}\int_0^1 f(r,\theta)\left[E_{pq}(r,\theta)\right]^* r dr d\theta \tag{1}$$

where the order and repetition, are $p = q = 0, \pm1, \pm2, \pm3, \ldots;$ $\hat{i} = \sqrt{-1};$ $[\cdot]^*$ the complex conjugate;$E_{pq}(r,\theta)$ refers to the exponent basis functions, which defined as:

$$E_{pq}(r,\theta) = T_p(r)\, e^{-\hat{i}q\theta} \tag{2}$$

With

$$T_p(r) = \sqrt{\frac{2}{r}} e^{-\hat{i}2\pi pr} \tag{3}$$

We generalized $E_{pq}(r,\theta)$ of integer orders in the domain $[0, 1] \times [0, 2\pi]$ and converted to the fractional-order form, $W^{\alpha}_{pq}(r,\theta)$, with a real-values parameter $\alpha \in \mathrm{R}^+$ in the same domain as follows:

$$W^{\alpha}_{pq}(r,\theta) = T_p(r,\alpha)\, e^{-\hat{i}q\theta} \tag{4}$$

where:

$$T_p(r,\alpha) = r^{\alpha-1}\sqrt{\frac{2}{r^{\alpha}}} e^{-\hat{i}2\pi pr^{\alpha}} \tag{5}$$

The basic functions of fractional-order, $\mathrm{W}^{\alpha}_{\mathrm{pq}}(\mathrm{r},\theta)$, are orthogonal where:

$$\int_0^{2\pi}\int_0^1 W^{\alpha}_{pm}(r,\theta)\left[W^{\alpha}_{qn}(r,\theta)\right]^* r dr d\theta = \frac{4\pi}{\alpha}\delta_{pm}\delta_{qn} \tag{6}$$

Based on the advantages of the multi-channel approach [36], [37] over the quaternion approach, the input color images represented using the RGB color model where the R, G & B channels are expressed using $g_R(r,\theta)$, $g_G(r,\theta)$ & $g_B(r,\theta)$, respectively. The multi-channel orthogonal fractional-order exponent moments are:

$$FrM_{pq} = \frac{\alpha}{4\pi}\int_0^{2\pi}\int_0^1 g_c(r,\theta)\, r^{\alpha-1}\sqrt{\frac{2}{r^{\alpha}}} e^{-\hat{i}2\pi pr^{\alpha}} e^{-iq\theta} r dr d\theta \tag{7}$$

The image function, $g_C(r,\theta)$, reconstructed as:

$$\begin{aligned} g_C^{recons.}(r,\theta) &= \sum_{p=-\infty}^{\infty}\sum_{q=-\infty}^{\infty} FrM_{pq}(g_C) W^{\alpha}_{pq}(r,\theta) \\ &\approx \sum_{p=-pmax}^{pmax}\sum_{q=-qmax}^{qmax} FrM_{pq}(g_C) W^{\alpha}_{pq}(r,\theta) \end{aligned} \tag{8}$$

The reconstructed color image $g_C^{recons.}(r,\theta)$ obtained using $g_R^{recons.}(r,\theta)$, $g_G^{recons.}(r,\theta)$, and $g_B^{recons.}(r,\theta)$. The quality of the reconstructed image is improved as *pmax* & *qmax* increased.

B. GEOMETRIC INVARIANCE OF MFrEMs

Geometric invariant watermarking relies on the invariance to RST geometric transformations. Through the following subsections, we mathematically derive and prove the RST invariance.

1) ROTATION INVARIANCE

Let $g_C(r,\theta)$ refers to the original color image, then, the rotated image with an angle β is while $g_C^{\beta}(r,\theta)$, where:

$$g_C^{\beta}(r,\theta) = g_C(r,\theta-\beta) \tag{9}$$

The MFrEMs of $g_C^{\beta}(r,\theta)$ is

$$\begin{aligned} &FrM_{pq}^{R}\left(g_C^{\beta}\right) \\ &= \frac{\alpha}{4\pi}\int_0^{2\pi}\int_0^1 g_C^{\beta}(r,\theta)\left[W_{pq}(r,\theta)\right]^* r dr d\theta \\ &= \frac{\alpha}{4\pi}\int_0^{2\pi}\int_0^1 g_C(r,\theta-\beta)T_p(\alpha,r)e^{-iq\theta} r dr d\theta \\ &= \frac{\alpha}{4\pi}\int_0^{2\pi}\int_0^1 g_C(r,\theta)T_p(\alpha,r)e^{-iq(\theta+\beta)} r dr d\theta \\ &= \frac{\alpha}{4\pi}\int_0^{2\pi}\int_0^1 g_C(r,\theta)T_p(\alpha,r)e^{-iq\theta}e^{-iq\beta} r dr d\theta \\ &= FrM_{pq}(g_C)e^{-iq\beta} \end{aligned} \tag{10}$$

Simply, we could write:

$$FrM_{pq}\left(g_C^{\beta}\right) = e^{-iq\beta}FrM_{pq}(g_C), \quad C \in \{R,G,B\} \tag{11}$$

where $FrM_{pq}(g_C)$ and $FrM_{pq}(g_C^{\beta})$ are the MFrEMs of, $g_C(r,\theta)$ and $g_C^{\beta}(r,\theta)$, respectively.

Since $\left|e^{-iq\beta}\right| = 1$, for any value of q and β; therefore:

$$\left|FrM_{pq}\left(g_C^{\beta}\right)\right| = \left|e^{-iq\beta}FrM_{pq}(g_C)\right|$$

Then:

$$\left|FrM_{pq}\left(g_C^{\beta}\right)\right| = \left|FrM_{pq}(g_C)\right| \tag{12}$$

Equation (12) proves the rotation invariance of MFrEMs.

2) SCALING INVARIANCE

The scaling invariance of the multi-channels orthogonal circular moments is valid if these circular moments are computed in polar coordinates [38]. In the proposed method, the MFrEMs are defined and calculated on the unit circle where input RGB color images are mapped. (See Fig. 1).

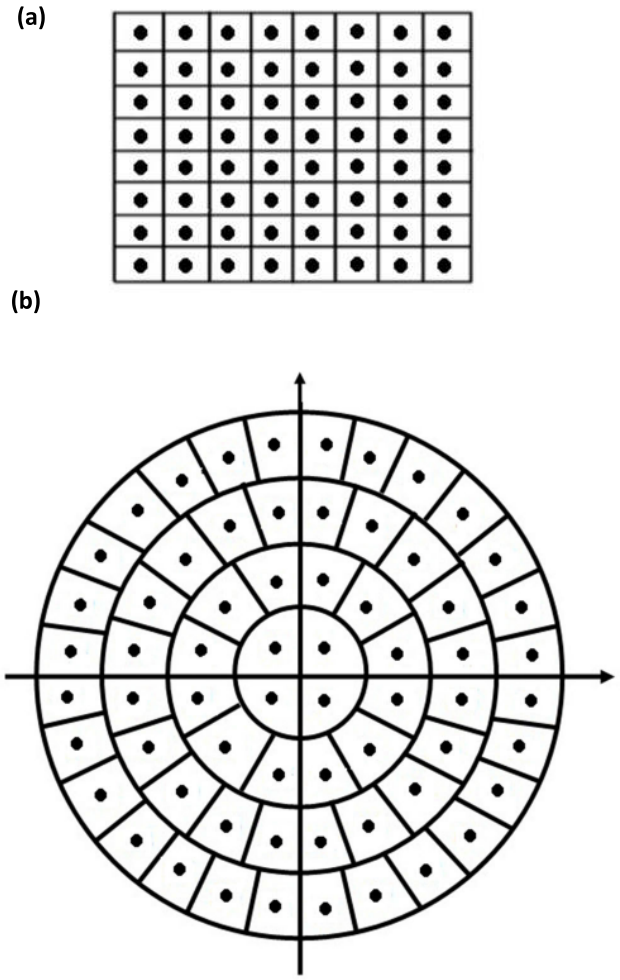

FIGURE 1. Cartesian to Polar mapping: (a) Cartesian pixels, (b) Polar pixels.

3) TRANSLATION INVARIANCE

Invariance to translation means shifting the coordinate origin to coincides with image centroid (x_c, y_c) [39] where x_c & y_c defined using geometric moments as:

$$\begin{aligned} x_c &= \left(m_{10}(g_R) + m_{10}(g_G) + m_{10}(g_B)\right)/m_{00}, \\ y_c &= \left(m_{01}(g_R) + m_{01}(g_G) + m_{01}(g_B)\right)/m_{00}, \\ m_{00} &= m_{00}(g_R) + m_{00}(g_G) + m_{00}(g_B). \end{aligned} \tag{13}$$

The central MFrEMs are:

$$\begin{aligned} \overline{FrM}_{pq} &= \frac{\alpha}{4\pi}\int_0^{2\pi}\int_0^1 g_C(\bar{r},\bar{\theta})\left[W_{pq}(\bar{r},\bar{\theta})\right]^* \bar{r} d\bar{r} d\bar{\theta} \\ &= \frac{\alpha}{4\pi}\int_0^{2\pi}\int_0^1 g_C(\bar{r},\bar{\theta})T_p(\alpha,\bar{r})e^{-iq\bar{\theta}}\bar{r} d\bar{r} d\bar{\theta} \end{aligned} \tag{14}$$

C. ACCURATE COMPUTATION OF MFrEMs

Accurate computation of MFrEMs is the cornerstone of the proposed watermarking algorithm. The accumulations of both geometrical and numerical errors degrade the process of watermarking and significantly decrease the robustness of

the watermarking against various attacks. The highly accurate kernel-based approach [40] utilized where the MFrEMs are computed as follows:

$$FrM_{pq} = \frac{\alpha}{4\pi} \sum_{i} \sum_{j} K_{pq}\left(r_i, \theta_{ij}\right) \hat{g}_C\left(r_i, \theta_{i,j}\right) \tag{15}$$

with

$$K_{pq}\left(r_i, \theta_{ij}\right) = I_p\left(r_i\right) J_q\left(\theta_{ij}\right) \tag{16}$$

We applied the cubic interpolation [41] to get the interpolated color image, $\hat{\boldsymbol{g}}_{\boldsymbol{C}}\left(\boldsymbol{r_i}, \boldsymbol{\theta_{i,j}}\right)$. The angular and radial kernels are defined as:

$$J_q\left(\theta_{ij}\right) = \int_{V_{ij}}^{V_{i,j+1}} e^{-\hat{i}q\theta} d\theta \tag{17}$$

$$I_P\left(r_i\right) = \int_{U_i}^{U_{i+1}} T_p(\alpha, r) r dr = \int_{U_i}^{U_{i+1}} R(r) dr \tag{18}$$

With:

$$R\left(r\right) = T_p(\alpha, r) r \tag{19}$$

The limits, $\boldsymbol{V_{i,j+1}}$, $\boldsymbol{V_{i,j}}$, $\boldsymbol{U_{i+1}}$ & $\boldsymbol{U_i}$ are:

$$V_{i,j+1} = \theta_{i,j} + \Delta\theta_{i,j}/2; \quad V_{i,j} = \theta_{i,j} - \Delta\theta_{i,j}/2 \tag{20}$$

$$U_{i+1} = R_i + \Delta R_i/2; \quad U_i = R_i - \Delta R_i/2 \tag{21}$$

Based on the principles of Calculus, $J_q\left(\theta_{ij}\right)$ computed in the exact form

$$J_q\left(\theta_{i,j}\right) = \begin{cases} \frac{\hat{i}}{q}\left(e^{-\hat{i}qV_{i,j+1}} - e^{-\hat{i}qV_{i,j}}\right), & q \neq 0 \\ V_{i,j+1} - V_{i,j}, & q = 0 \end{cases} \tag{22}$$

Unlike $\boldsymbol{J_q}\left(\boldsymbol{\theta_{ij}}\right)$, calculating $\boldsymbol{I_p}\left(\boldsymbol{r_i}\right)$; requires numerical integration. Based on its successful implementation in [42], [43], accurate Gaussian integration [44] is our choice. The $\boldsymbol{I_p}\left(\boldsymbol{r_i}\right)$ computed using as:

$$I_p\left(r_i\right) = \int_{U_i}^{U_{i+1}} R\left(r\right) dr \approx \frac{\left(U_{i+1} - U_i\right)}{2} \sum_{l=0}^{c-1} w_l \times R\left(\frac{U_{i+1} + U_i}{2} + \frac{U_{i+1} - U_i}{2} t_l\right) \tag{23}$$

The symbols, w_l & t_l, refer to weights and the locatio $l = 0, 1, 2, \ldots . c - 1$ of sampling points; c is the order of the numerical integration. The values of w_l are fixed and $\sum_{l=0}^{c-1} w_l = 2$. The values of t_l can be expressed in terms of the limits of the integration U_i and U_{i+1}.

For an efficient computational process, the 8-point symmetry is applied where the moments' computation is performed using the first octant. Fig. 1 shows that the red and blue colored pixels refer to the first and second kind of symmetry in the polar raster. Each red pixel in the first octant has 7 similar pixels in the 2nd to 8th octants, while each blue-pixel has 3 similar pixels on the diagonals.

III. PROPOSED WATERMARKING SCHEME

The MFrEMs are combined with a 1D Sine map to design a new watermarking algorithm for color images. In this algorithm, we selected RST invariants MFrEMs magnitudes and used these selected moments to construct a robust watermark. Then, we used a sine map in scrambling the image features. Through the following subsection, we consider the host color image, g_c, of size $N \times N$ while the watermark is a binary image, W, of size $P \times Q$ where $W = \{w\left(i, j\right) \in \{0, 1\}, 0 \leq i < P, 0 \leq j < Q\}$.

A. EMBEDDING PROCESS

The embedding process is achieved through three steps. First, the MFrEMs of the host color image are computed. Second, the most significant TSR MFrEMs invariant selected. Third, the bits of the watermark embedded in the selected moment invariants. Fig. 2 shows an illustrated flowchart of the embedding process.

Step 1: Transforming and Scrambling the binary watermark image.

The watermark image, W, is converted to a one-dimensional vector, W_1, where $W_1 = \{w_1\left(i\right) : 0 \leq i < P \times Q\}$. Then a chaotic sequence C of the length P × Q generated by using the Sine chaotic map [45] with the initial value of x_0. This map defined as follows:

$$x_{n+1} = rsin(\pi x_n) \tag{24}$$

The variable r is the control parameter of the Sine map, $r \in [0, 1]$. The chaotic sequence $C = \{c\left(i\right) : 0 \leq i < P \times Q\}$ can be obtained using key K_1 as the initial value of the Sine chaotic mapping, where the initial value of the Sine chaotic mapping watermark sequence scrambled using Sine chaotic mapping and a binarized chaotic sequence $\hat{C} = \{\hat{c}(i), 0 \leq i < P \times Q\}$ is obtained by binarizing C as follows:

$$\hat{C}(i) = \begin{cases} 1, & if\ \hat{c}\left(\mathrm{i}\right) \geq T \\ 0, & if\ \hat{c}(\mathrm{i}) < T, \end{cases} \quad (0 \leq \mathrm{i} < \mathrm{P} \times \mathrm{Q})$$

where T refers to the threshold, which is defined as the mean of C. Then, the binarized watermark sequence is scrambled from W_1 to $\hat{W}_1$ by applying the XOR logical operation on the watermark sequence and the binarized chaotic sequence $\hat{C}$, and a chaotic scrambled watermark sequence, $\hat{W}_1 = \{\hat{w}_1(i), 0 \leq i < P \times Q\}$, is generated:

$$\hat{W}_1 = XOR(W_1, \hat{C}) \tag{25}$$

Step 2: Computing MFrEMs

The scaling and translation invariants of MFrEMs for the host image are computed according to a maximum moment order equal to $P \times Q$.

Step 3: Selected MFrEMs

The magnitude values of MFrEMs are computed to assure the invariances. Xin *et al.* [10] in their remarkable work showed that orthogonal moments in circular domain with $q = 4m$, $m \in Z$ (i.e., m = 0, m = 4, m = 8, m = 12, ...) are not suitable to embed the watermark bits. The

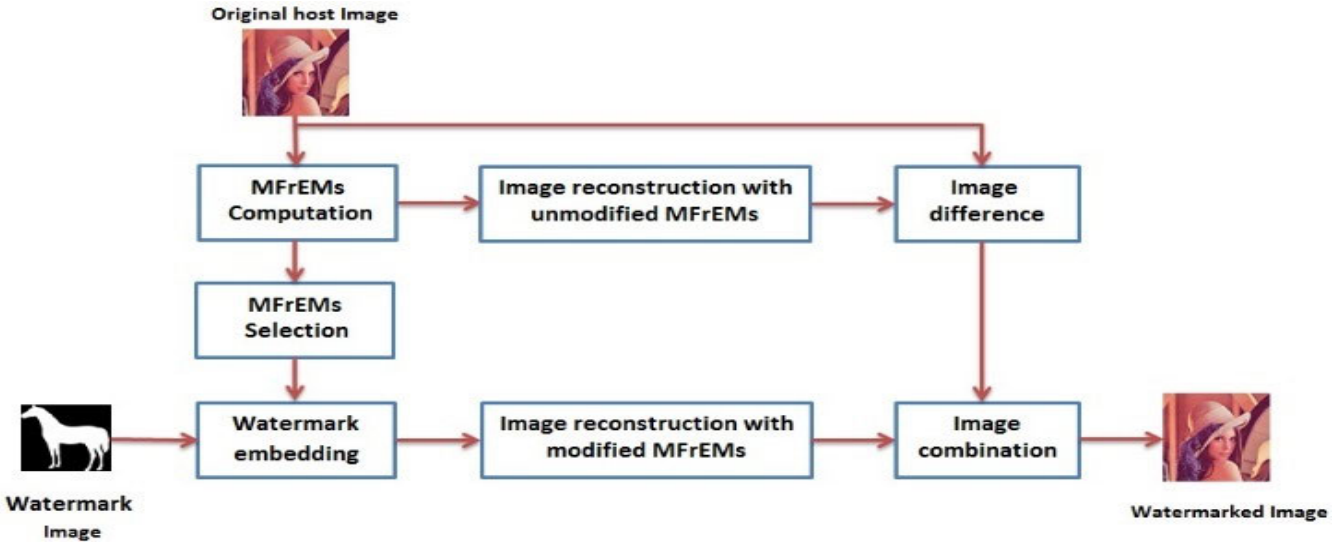

FIGURE 2. Watermark embedding framework.

FIGURE 3. Watermark extraction framework.

dependence of the MFrEMs with negative repetition m < 0 on the MFrEMs with positive repetition m > 0 results in an information redundancy. Therefore, we select MFrEMs with positive repetitions, $q \neq 4m$, $m \in Z$, as follows:

$$S = \{\left|FrM_{pq}\right|, q \neq 4m,\ m \in Z\}$$

By using a secret key K_2, $P \times Q$ coefficients MFrEMs, M_{FrEM}, are randomly selected from the accurate coefficients set S based on the number of digital watermark bits, and the magnitudes sequence of the feature vector are obtained.

Step 4: Watermark embedding

The binary watermark bits embedded in the host color image modulate selected MFrEMs using the dither modulation function [10].

$$m'_{FrEM}(\mathrm{i}) = \left[\frac{m_{FrEM}(\mathrm{i}) - \mathrm{d_i}(\hat{\mathrm{w}}_1(\mathrm{i}))}{\Delta}\right] * \Delta + \mathrm{d_i}\left(\hat{\mathrm{w}}_1(\mathrm{i})\right), \quad 0 \leq \mathrm{i} < \mathrm{P} \times \mathrm{Q}$$
$$d_i(1) = \frac{\Delta}{2} + d_i(0), \quad d_i(0) \in [0, 1] \tag{26}$$

where $m_{FrEM}(\mathrm{i})$ refers to a vector that contains these magnitude values of selected MFrEMs. The vector length is equal to the number of watermark bits; $m'_{FrEM}(\mathrm{i})$ refers to the modulated one; the $[\cdot]$ is the rounding operator; Δ refers to watermark quantization step; $\mathrm{d_i}$ refers to the dither function where dither vector elements are uniformly distributed over $[0, \Delta]$ and randomly generated.

Step 5: Obtaining the watermarked image

The inverse operation of MFrEMs is applied to obtain the watermarked color image, $\boldsymbol{g_c^w}(\boldsymbol{r}, \boldsymbol{\theta})$, as:

$$g_c^w(r, \theta) = g_c(r, \theta) - g_c^M(r, \theta) + g_c^{M'}(r, \theta) \tag{27}$$

where $\boldsymbol{g_c}(\boldsymbol{r}, \boldsymbol{\theta})$ denotes the original image, $\boldsymbol{g_c^M}(\boldsymbol{r}, \boldsymbol{\theta})$ & $\boldsymbol{g_c^{M'}}(\boldsymbol{r}, \boldsymbol{\theta})$, are the image components contributed by using unmodified and modified MFrEMs, respectively.

B. WATERMARK EXTRACTION PROCESS

The extraction process is an inverse process of the embedding one, where the binary bits of the watermark is extracted. First, the MFrEMs are computed for the watermarked image using the same accurate method. Second, a similar selection process is applied. Third, the same secret keys are employed. Finally, the binary watermark bits are extracted. Fig. 3 shows a flowchart for the extraction process.

Step 1: Computing MFrEMs moments of the attacked watermarked image

The MFrEMs of this image is calculated using the same accurate method as described in Section II-C.

Step 2: Selected MFrEMs Coefficients

The $P \times Q$ feature vector of MFrEMs, $M^*_{FrEM} = \left\{m^*_{FrEM}(i), 0 \le i < P \times Q\right\}$ are selected by using the same secret key, K_2, which is a symmetric key for the embedding and extraction processes.

Step 3: Extraction of the watermark sequence

The selected MFrEMs magnitudes are extracted using the same quantization process as:

$$\left|m^*_{FrEM}(i)\right|_j = \left[\frac{\left|m^*_{FrEM}\right| - d_i(j)}{\Delta}\right] * \Delta + d_i(j), \quad j = 0, 1 \tag{28}$$

A bit $\hat{w}^*_1(i)$ is either 0 or 1 based on the value $m^*_{FrEM}(i)$ where:

$$\hat{w}^*_1(i) = \underset{j\in[0,1]}{\operatorname{argmin}} \left(\left|m^*_{FrEM}(i)\right|_j - \left|m^*_{FrEM}(i)\right|\right)^2 \tag{29}$$

The $\hat{w}^*_1(i)$ is called a minimum distance decoder.

Step 4: Generation of the watermark image

The one-dimensional watermark, W^*_1, is obtained by performing reverse Sine mapping and scrambling of $\hat{W}^*_1 = \{\hat{w}^*_1(i), 0 \le i < P \times Q\}$ using key K_1. Then, $W^*_1 = \{w^*_1(i), 0 \le i < P \times Q\}$ is transformed into a two-dimensional binary watermark $W^* = \{w^*(i, j) \in \{0, 1\}, 0 \le i < P, 0 \le j < Q\}$.

IV. EXPERIMENTS

Few experiments are performed to test the proposed watermarking algorithm and compare its performance with recent existing algorithms [17]–[20] using quantitative and qualitative measures: visual imperceptibility the robustness against attacks are used as metrics for watermarking performance. Several criteria are used to qualify the proposed method; visual imperceptibility was evaluated by Peak Signal-to-Noise Ratio (PSNR) as a quantitative measure. Robustness against attacks measured using the Normalized Correlation (NC) and the bit error rate (BER) as quantitative measures. In the experiments, eight standard color images, as displayed in Fig. 4, are selected and used as host images. Eight binary images, as shown in Fig. 4 used as test watermarks.

FIGURE 4. Standard Color images (Host images).

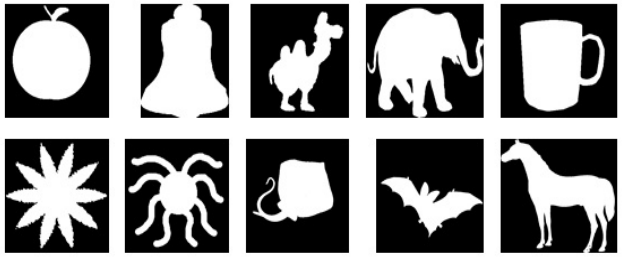

FIGURE 5. Binary images (watermarks).

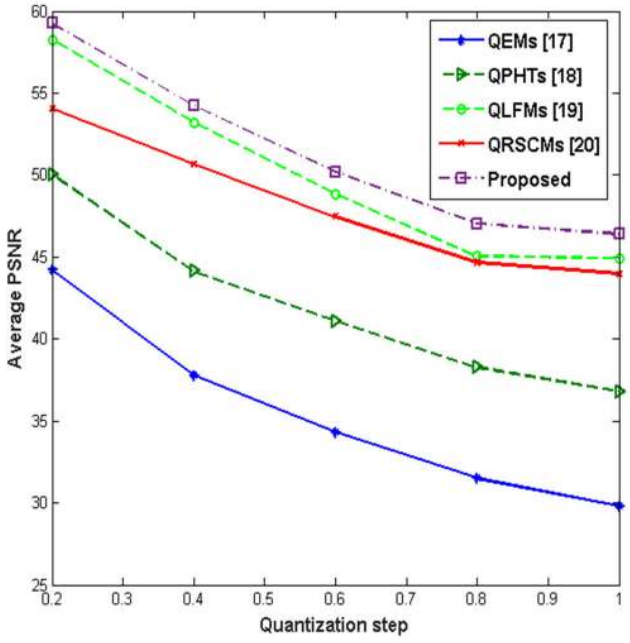

FIGURE 6. PSNR using different values of (Δ).

A. WATERMARK INVISIBILITY

Excellent watermark imperceptibility means an invisible watermark. In other words, the human eye cannot see the embedded watermark. The PSNR value is an indicator of imperceptibility, where increased PSNR means improved imperceptibility.

The PSNR of the watermarked image, g^w_c, and the original image, g_c, is:

$$PSNR\left(g_c, g^w_c\right) = 10\log_{10}\frac{255^2}{MSE} \tag{30}$$

where:

$$MSE = \frac{1}{N^2}\left(\sum_{i=1}^{N}\sum_{j=1}^{N}\left[g^w_c(i,j) - g_c(i,j)\right]^2\right) \tag{31}$$

Since various positive real numbers could be assigned to the fractional parameter $\alpha \in R^+$, we must precisely determine the best choice. To achieve this goal, the authors theoretically analyzed the behavior of the real-values radial function, $T_p(r, \alpha)$, using various values of α; some of these values are less than 1, and the others are greater than 1. Xiao *et al.* [28] showed that $0 < \alpha < 2$.

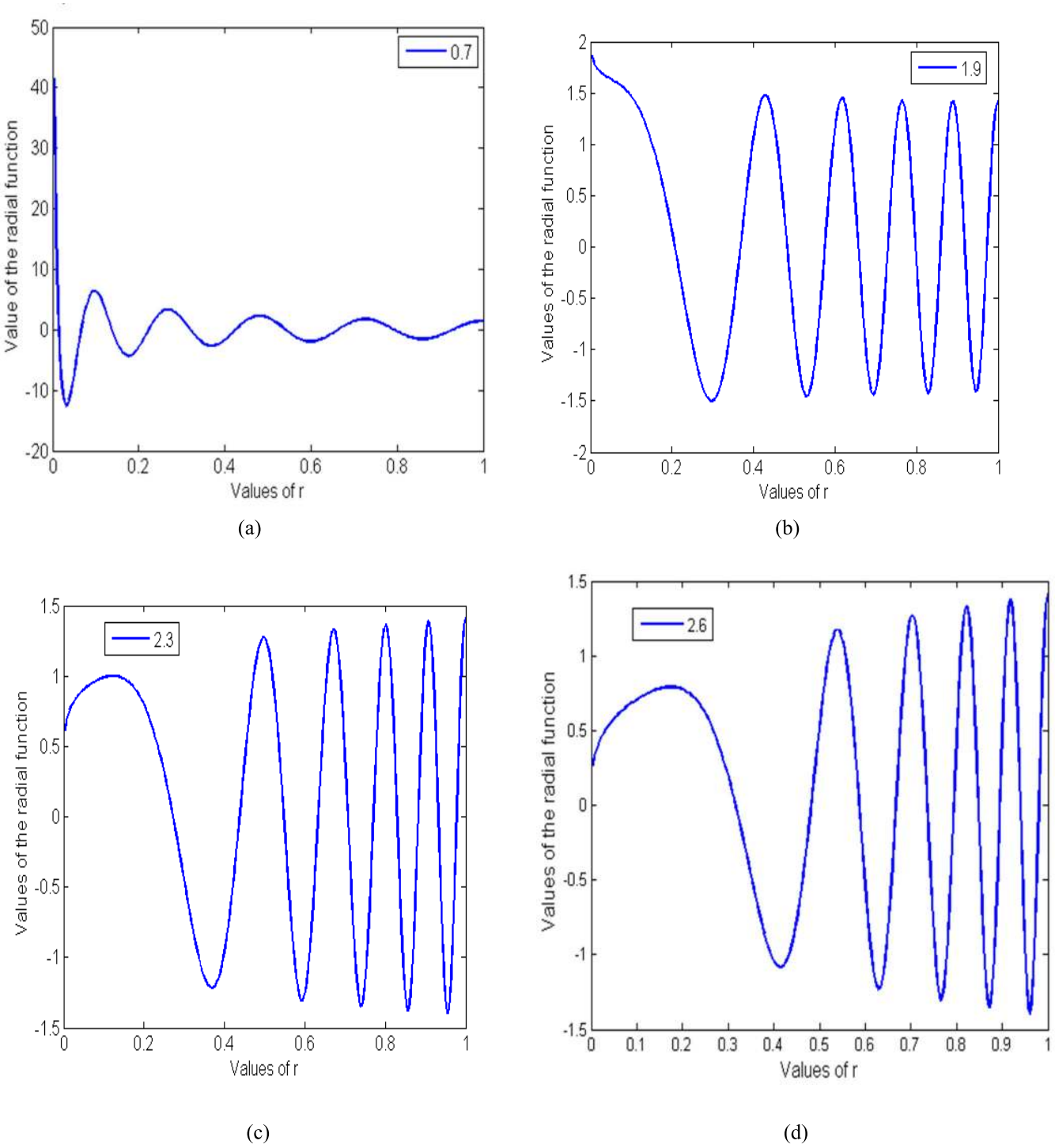

FIGURE 7. Real-values radial function using the order $p = 10$: (a) MFrEMs with $\alpha = 0.7$, (b) MFrEMs with $\alpha = 1.9$, (c) MFrEMs with $\alpha = 2.3$, (d) MFrEMs with $\alpha = 2.6$.

Accordingly, we used various values of the parameter α (0.7, 1.9, 2.3, and 2.6) and then plotted the curves corresponding to these values. The plotted curves are displayed in Fig. 7(a) to 7(d). For $\alpha = 0.7$, the plotted curve shows high fluctuations, which makes this selection unacceptable. Despite the reduction of fluctuations with $\alpha = 2.3$ & $\alpha = 2.6$, the radial function is non-uniformly distributed and tends to be concentrated at the outer region of the circular domain. On the other side, the value $\alpha = 1.9$ represents the best choice where no fluctuations and the radial function is uniformly distributed over the entire domain ($0 \leq r \leq 1$). An additional experiment is performed to confirm this observation. The standard color image of Lena is reconstructed using the MFrEMs with $\alpha = 0.7$, 1.9, 2.3, and 2.6. The reconstructed

TABLE 1. The average PSNR (dB) using different amounts of (Δ).

Quantization step	QEMs [17]	QPHTs [18]	QLFMs [19]	QRSCMs [20]	Proposed Algorithm
0.2	44.20	50.03	58.25	54.03	59.27
0.4	37.78	44.12	53.21	50.67	54.24
0.6	34.31	41.08	48.86	47.46	50.21
0.8	31.51	38.25	45.05	44.67	47.05
1.0	29.81	36.78	44.91	43.97	46.41

TABLE 2. Average values of BER with various attacks.

Various Attacks		QEMs [17]	QPHTs [18]	QLFMs [19]	QRSCMs [20]	Proposed Method
Rotation Angle	5°	0.014	0.0115	0	0	0
	15°	0.007	0.0135	0	0	0
	25°	0.013	0.0170	0	0	0
	35°	0.008	0.0201	0	0	0
	45°	0.009	0.0285	0	0	0
Scaling Factor	0. 5	0.076	0.4377	0.035	0.051	0.0036
	0.75	0.021	0.0896	0	0	0
	1.25	0.0098	0.0267	0	0	0
	1.75	0	0.0098	0	0	0
	2.0	0	0.0145	0	0	0
Translation	(V15, H2)	0.0025	0.0135	0	0	0
	(V20, H20)	0.0048	0.0402	0.0025	0.0039	0.0003
	(V2, H15)	0.0039	0.0138	0	0	0
	(V0, H50)	0.0048	0.0148	0.0018	0.0029	0.0002
	(V50, H0)	0.0098	0.0151	0.0048	0.0058	0.0001
Compression	JPEG, 30%	0.0405	0.0683	0.0135	0.0247	0.0029
	JPEG, 40%	0.0236	0.0189	0.0068	0.0098	0
	JPEG, 50%	0.003	0.0134	0	0	0
	JPEG, 70%	0.001	0.0125	0	0	0
	JPEG, 90%	0	0.0107	0	0	0
Shearing (0%-1%)		0.0352	0.0105	0.0085	0.0098	0.0003
Magnification (1.75) + JPEG (90%)		0.0173	0.0001	0	0	0.
Noise (Gaussian, 0.03) + JPEG (90%)		0.0268	0.0005	0.0006	0.0009	0
Rotation (35°) + JPEG (90%)		0.0226	0.0002	0	0	0
Translation (V2, H5) + Noise "Salt& Peppers, 0.03"		0.0346	0.0078	0.0029	0.0068	0.0003
Noise "Salt& Peppers, 0.03"		0.0165	0.0251	0.0005	0.0007	0
Noise (Gaussian, 0.01)		0.0184	0.0465	0.0009	0.0013	0
Filtering (Median, 3×3)		0.0215	0.0068	0.0039	0.0058	0.0004

images are displayed in Fig. 8. The quantitative and qualitative measures of the reconstructed images show that $\alpha = 1.9$ is the best choice.

The imperceptibility of the proposed watermark algorithm was evaluated in the first experiment. The MFrEMs are computed with $\alpha = 1.9$. The proposed and the existing algorithms [17]–[20] used to embed a 128-bit watermark sequence into the eight standard color images with $\Delta \in [0.2, 0.4, 0.6, 0.8, 1.0]$. Fig. 6 clearly shows that the average PSNR is decreased as the value of Δ is increased. Also,

TABLE 3. Binary watermark extraction with various distortions.

Attacks		QEMs [17]	QPHTs [18]	QLFMs [19]	QRSCMs [20]	Proposed Method
Rotation angle	15 °					
	35 °					
	45 °					
Scaling factor	0.75					
	1.5					
	2					
Translation	(H 3, V 3)					
	(H 6, V 6)					
Magnification (1.75) + Rotation (25°)						
Reduction (0.75) + JPEG compression (90%)						
Magnification (1.5) + Compression (JPEG, 90%)						
Rotation (25°) + Compression (JPEG, 90%)						
compression	(JPEG, 80%)					
	(JPEG, 90%)					
Noise "Salt & Peppers, 0.03"						
Noise "Gaussian, 0.03"						
Filtering (Gaussian, 3*3)						
Filtering (Median, 3*3)						

the value $\Delta = 0.2$ results in the highest average PSNR; therefore, we used this value, $\Delta = 0.2$, in all the performed experiments.

Each standard image is watermarked using the eight binary watermarks of 32×32; therefore, the proposed watermarking

TABLE 4. BER values distorted watermark.

Various Attacks		QEMs [17]	QPHTs [18]	QLFMs [19]	QRSCMs [20]	Proposed Method
Rotation angle	15 °	0.0703	0.1582	0.0479	0.0479	0.0195
	35 °	0.0557	0.1533	0.0361	0.0449	0.0176
	45 °	0.0547	0.1514	0.0459	0.0459	0.0195
Scaling factor	0.75	0.0781	0.1377	0.0469	0.0518	0.0166
	1.5	0.0283	0.0898	0.0098	0.0127	0.0049
	2	0.0322	0.0586	0.0078	0.0205	0.0039
Shift (Translation)	(H 3, V 3)	0.0186	0.0625	0.0205	0.0107	0.0039
	(H 6, V 6)	0.0479	0.0635	0.0215	0.0205	0.0049
Magnification (1.75) + Rotation (25°)		0.1699	0.0342	0.0215	0.0244	0.0049
Reduction (0.75) + Compression (JPEG, 90%)		0.1064	0.0557	0.0205	0.0215	0.0107
Magnification (1. 5) + Compression (JPEG, 90%)		0.0889	0.0293	0.0107	0.0127	0.0049
Rotation (25°) + ompression (JPEG, 90%)		0.1406	0.0742	0.0459	0.0566	0.0195
Compression	(JPEG, 80%)	0.0205	0.0859	0.0127	0.0186	0.0059
	(JPEG, 90%)	0.0107	0.0693	0.0029	0.0049	0.0039
Noise, "Salt & Peppers, 0.03"		0.084	0.0166	0.0146	0.0156	0.0068
Noise, "Gaussian, 0.03"		0.0723	0.0293	0.0107	0.0186	0.0039
Filtering (Gaussian, 3*3)		0.1006	0.0166	0.0127	0.0146	0.0049
Filtering (Median, 3*3)		0.0859	0.0342	0.0137	0.0283	0.0068

TABLE 5. NC values of distorted watermarks.

Attacks		QEMs [17]	QPHTs [18]	QLFMs [19]	QRSCMs [20]	Proposed Method
Rotation angle	15 °	0.9143	0.7850	0.9409	0.9408	0.9759
	30 °	0.9316	0.7941	0.9551	0.9445	0.9782
	45 °	0.9322	0.7945	0.9439	0.9434	0.9758
Scaling factor	0.75	0.9048	0.8146	0.9424	0.9374	0.9794
	1.5	0.9652	0.8825	0.9880	0.9843	0.9940
	2	0.9605	0.9251	0.9904	0.9745	0.9952
Shift	(H 3, V 3)	0.9770	0.9237	0.9745	0.9867	0.9952
	(H 6, V 6)	0.9412	0.9226	0.9736	0.9747	0.9940
Magnification (1.75) + Rotation (25°)		0.7677	0.9582	0.9737	0.9697	0.9940
Reduction (0.75) + Compression (JPEG, 90%)		0.8591	0.9319	0.9745	0.9736	0.9867
Magnification (1.5) + Compression (JPEG, 90%)		0.8880	0.9643	0.9867	0.9843	0.9940
Rotation (25°) + Compression (JPEG, 90%)		0.8136	0.9103	0.9439	0.9306	0.9758
Compression	(JPEG, 80%)	0.9745	0.8839	0.9843	0.9769	0.9928
	(JPEG, 90%)	0.9867	0.9107	0.9964	0.9940	0.9952
Noise, "Salt & Peppers, 0.03"		0.8907	0.9794	0.9820	0.9806	0.9916
Noise, "Gaussian, 0.03"		0.9067	0.9643	0.9867	0.9769	0.9952
Filtering (Gaussian, 5*5)		0.8674	0.9794	0.9843	0.9820	0.9940
Filtering (Median ,5*5)		0.8953	0.9582	0.9831	0.9650	0.9916

algorithm is tested using 64 watermarked images. The average PSNR values are computed for all compared algorithms and plotted in Fig. 6. The PSNR values are decreased as the quantization step is increased. Table 1 shows the average values of PSNR computed using different algorithms [17]–[20]. As observed in Fig. 6 and Table 1, the proposed watermarking algorithm achieved the highest values of PSNR, where all PSNR values are greater than 44 dB, which means that the proposed scheme achieved the imperceptibility requirements. The proposed algorithm outperformed the existing algorithms [17]–[20].

Based on (32) and (33), NC and BER's optimum values are 1 and 0.

An additional experiment is conducted to assess the robustness against various attacks. A binary watermark image is resized to 10×10 and embedded into the host images using the proposed algorithm with $\alpha = 1.9$, and the existing watermarking methods [17]–[20]. We reconstructed 64 watermarked color images for each algorithm and then applied various attacks to distort each of the watermarked images. The embedded watermark is extracted. The average BER values for each method are computed and presented in Table 2, which shows that the new MFrEMs-based watermarking algorithm provides the most robustness for different attacks.

Tables 4 and 5 show the BER and NC values of the extracted watermarks using the proposed algorithm and the algorithms [17]–[20]. The smallest values in Table 4, while the highest values in Table 5, show the new MFrEMs-based watermarking algorithm's superiority over the algorithms [17]–[20].

B. ROBUSTNESS OF THE WATERMARK

The robustness against the attacks is evaluated using the BER and NC measures, which are defined as:

$$BER = \frac{1}{P \times Q}\left(\sum_{i=1}^{P}\sum_{j=1}^{Q}\left[w(i,j) - w^*(i,j)\right]^2\right) \quad (32)$$

$$NC = \frac{\sum_{i=1}^{P}\sum_{j=1}^{Q}\left[w(i,j) \times w^*(i,j)\right]}{\sum_{i=1}^{P}\sum_{j=1}^{Q}\left[w(i,j)\right]^2} \quad (33)$$

FIGURE 8. Reconstructed color images of Lena.

The symbols, W & W^*, refer to the original and extracted watermarks.

An additional experiment is conducted using the binary CUP image of size 32×32, embedded in Lena's color image using the new MFrEMs-based method and the algorithms in [17]–[20]. The reconstructed watermarked color image is distorted using different attacks, and then the extracted CUP watermarks are presented in Table 3. For simplicity, the corresponding BER and NC for each extracted watermark are computed and presented in Tables 4 and 5, respectively. Table 3 shows that the extracted watermarks by the proposed algorithm recognized after these attacks.

V. CONCLUSION

A new algorithm was proposed for robust watermarking of color images. This algorithm is based on new fractional-order multi-channel moments. These MFrEMs are accurate and stable, where higher-order moments are calculated with minimum numerical errors. A 1D Sine chaotic map is used to scramble the binary watermarks' bits where these scrambled bits are embedded into host color images by adapting the MFrEMs magnitudes. Simple attacks and a complicated combination of different attacks are applied to the color watermarked images. Despite these attacks, the extracted embedded watermarks are very similar to the original watermarks. Numerical simulation ensures the embedded watermark's high invisibility and robustness against different kinds of geometric distortions and attacks. Also, the proposed algorithm outperforms the existing algorithms.

REFERENCES

[1] X. Qi and J. Qi, "A robust content-based digital image watermarking scheme," *Signal Process.*, vol. 87, no. 6, pp. 1264–1280, Jun. 2007.
[2] A. Cedillo-Hernandez, M. Cedillo-Hernandez, M. N. Miyatake, and H. P. Meana, "A spatiotemporal saliency-modulated JND profile applied to video watermarking," *J. Vis. Commun. Image Represent.*, vol. 52, pp. 106–117, Apr. 2018.
[3] X.-B. Kang, F. Zhao, G.-F. Lin, and Y.-J. Chen, "A novel hybrid of DCT and SVD in DWT domain for robust and invisible blind image watermarking with optimal embedding strength," *Multimedia Tools Appl.*, vol. 77, no. 11, pp. 13197–13224, 2018.
[4] P.-Y. Lin, J.-S. Lee, and C.-C. Chang, "Protecting the content integrity of digital imagery with fidelity preservation," *ACM Trans. Multimedia Comput., Commun., Appl.*, vol. 7, no. 3, pp. 1–20, Aug. 2011.
[5] C. Qin, P. Ji, X. Zhang, J. Dong, and J. Wang, "Fragile image watermarking with pixel-wise recovery based on overlapping embedding strategy," *Signal Process.*, vol. 138, pp. 280–293, Sep. 2017.
[6] S. Fazli and M. Moeini, "A robust image watermarking method based on DWT, DCT, and SVD using a new technique for correction of main geometric attacks," *Optik Int. J. Light Electron Opt.*, vol. 127, no. 2, pp. 964–972, 2016.
[7] C.-P. Wang, X.-Y. Wang, and Z.-Q. Xia, "Geometrically invariant image watermarking based on fast radial harmonic Fourier moments," *Signal Process. Image*, vol. 45, pp. 10–23, Jul. 2016.
[8] M. Alghoniemy and A. H. Tewfik, "Geometric distortion correction through image normalization," in *Proc. IEEE Int. Conf. Multimedia Expo*, New York, NY, USA, Aug. 2000, pp. 1291–1294.
[9] X.-C. Yuan, C.-M. Pun, and C.-L.-P. Chen, "Geometric invariant watermarking by local Zernike moments of binary image patches," *Signal Process.*, vol. 93, no. 7, pp. 2087–2095, Jul. 2013.
[10] Y. Xin, S. Liao, and M. Pawlak, "Circularly orthogonal moments for geometrically robust image watermarking," *Pattern Recognit.*, vol. 40, no. 12, pp. 3740–3752, Dec. 2007.
[11] L. Li, S. Li, A. Abraham, and J.-S. Pan, "Geometrically invariant image watermarking using polar harmonic transforms," *Inf. Sci.*, vol. 199, pp. 1–19, Sep. 2012.
[12] K. M. Hosny and M. M. Darwish, "Invariant image watermarking using accurate polar harmonic transforms," *Comput. Electr. Eng.*, vol. 62, pp. 429–447, Aug. 2017.
[13] E. D. Tsougenis, G. A. Papakostas, D. E. Koulouriotis, and E. G. Karakasis, "Adaptive color image watermarking by the use of quaternion image moments," *Expert Syst. Appl.*, vol. 41, no. 14, pp. 6408–6418, 2014.
[14] H.-Y. Yang, Y. Zhang, P. Wang, X.-Y. Wang, and C.-P. Wang, "A geometric correction based robust color image watermarking scheme using quaternion exponent moments," *Optik*, vol. 125, no. 16, pp. 4456–4469, Aug. 2014.
[15] P.-P. Niu, P. Wang, Y.-N. Liu, H.-Y. Yang, and X.-Y. Wang, "Invariant color image watermarking approach using quaternion radial harmonic Fourier moments," *Multimedia Tools Appl.*, vol. 75, no. 13, pp. 7655–7679, Jul. 2016.

[16] H.-Y. Yang, X.-Y. Wang, P.-P. Niu, and A.-L. Wang, "Robust color image watermarking using geometric invariant quaternion polar harmonic transform," *ACM Trans. Multimedia Comput., Commun., Appl.*, vol. 11, no. 3, pp. 1–26, Feb. 2015.
[17] X. Y. Wang, H. Y. Yang, P. P. Niu, and C. P. Wang, "Quaternion exponent moments based robust color image watermarking," *J. Comput. Res. Dev.*, vol. 53, no. 3, pp. 651–665, 2016.
[18] H. Xu, X. Kang, Y. Chen, and Y. Wang, "Rotation and scale invariant image watermarking based on polar harmonic transforms," *Optik*, vol. 183, pp. 401–414, Apr. 2019.
[19] K. M. Hosny and M. M. Darwish, "Robust color image watermarking using invariant quaternion Legendre-Fourier moments," *Multimedia Tools Appl.*, vol. 77, no. 19, pp. 24727–24750, Oct. 2018.
[20] K. M. Hosny and M. M. Darwish, "Resilient color image watermarking using accurate quaternion radial substituted Chebyshev moments," *ACM Trans. Multimedia Comput., Commun., Appl.*, vol. 15, no. 2, pp. 24727–24750, 2019.
[21] Z. Shao, Y. Shang, Y. Zhang, X. Liu, and G. Guo, "Robust watermarking using orthogonal Fourier–Mellin moments and chaotic map for double images," *Signal Process.*, vol. 120, pp. 522–531, Mar. 2016.
[22] C.-P. Wang, X.-Y. Wang, X.-J. Chen, and C. Zhang, "Robust zero-watermarking algorithm based on polar complex exponential transform and logistic mapping," *Multimedia Tools Appl.*, vol. 76, no. 24, pp. 26355–26376, Dec. 2017.
[23] Z. Xia, X. Wang, W. Zhou, R. Li, C. Wang, and C. Zhang, "Color medical image lossless watermarking using chaotic system and accurate quaternion polar harmonic transforms," *Signal Process.*, vol. 157, pp. 108–118, Apr. 2019.
[24] Z. Xia, X. Wang, X. Li, C. Wang, S. Unar, M. Wang, and T. Zhao, "Efficient copyright protection for three CT images based on quaternion polar harmonic Fourier moments," *Signal Process.*, vol. 164, pp. 368–379, Nov. 2019.
[25] B. Ma, L. Chang, C. Wang, J. Li, X. Wang, and Y.-Q. Shi, "Robust image watermarking using invariant accurate polar harmonic Fourier moments and chaotic mapping," *Signal Process.*, vol. 172, Jul. 2020, Art. no. 107544.
[26] B. Xiao, L. Li, Y. Li, W. Li, and G. Wang, "Image analysis by fractional-order orthogonal moments," *Inf. Sci.*, vols. 382–383, pp. 135–149, Mar. 2017.
[27] B. Chen, M. Yu, Q. Su, H. J. Shim, and Y.-Q. Shi, "Fractional quaternion Zernike moments for robust color image copy-move forgery detection," *IEEE Access*, vol. 6, pp. 56637–56646, 2018.
[28] B. Xiao, J. Luo, X. Bi, W. Li, and B. Chen, "Fractional discrete Tchebyshev moments and their applications in image encryption and watermarking," *Inf. Sci.*, vol. 516, pp. 545–559, Apr. 2020.
[29] K. M. Hosny, M. M. Darwish, and T. Aboelenen, "New fractional-order Legendre-Fourier moments for pattern recognition applications," *Pattern Recognit.*, vol. 103, Jul. 2020, Art. no. 107324.
[30] K. M. Hosny, M. M. Darwish, and M. M. Eltoukhy, "Novel multi-channel fractional-order radial harmonic Fourier moments for color image analysis," *IEEE Access*, vol. 8, pp. 40732–40743, 2020.
[31] K. M. Hosny, M. M. Darwish, and T. Aboelenen, "Novel fractional-order generic Jacobi-Fourier moments for image analysis," *Signal Process.*, vol. 172, Jul. 2020, Art. no. 107545.
[32] M. Yamni, H. Karmouni, M. Sayyouri, and H. Qjidaa, "Image watermarking using separable fractional moments of Charlier–Meixner," *J. Franklin Inst.*, vol. 358, no. 4, pp. 2535–2560, Mar. 2021, doi: 10.1016/j.jfranklin.2021.01.011.
[33] M. Yamni, A. Daoui, O. El Ogri, H. Karmouni, M. Sayyouri, H. Qjidaa, and J. Flusser, "Fractional Charlier moments for image reconstruction and image watermarking," *Signal Process.*, vol. 171, Jun. 2020, Art. no. 107509.
[34] B. Chen, C. Zhou, B. Jeon, Y. Zheng, and J. Wang, "Quaternion discrete fractional random transform for color image adaptive watermarking," *Multimedia Tools Appl.*, vol. 77, no. 16, pp. 20809–20837, Aug. 2018.
[35] H.-T. Hu, Y.-D. Zhang, C. Shao, and Q. Ju, "Orthogonal moments based on exponent functions: Exponent-Fourier moments," *Pattern Recognit.*, vol. 47, no. 8, pp. 2596–2606, Aug. 2014.
[36] C. Singh and J. Singh, "Multi-channel versus quaternion orthogonal rotation invariant moments for color image representation," *Digit. Signal Process.*, vol. 78, pp. 376–392, Jul. 2018.
[37] K. M. Hosny and M. M. Darwish, "New set of multi-channel orthogonal moments for color image representation and recognition," *Pattern Recognit.*, vol. 88, pp. 153–173, Apr. 2019.
[38] X.-Y. Wang, W.-Y. Li, H.-Y. Yang, P. Wang, and Y.-W. Li, "Quaternion polar complex exponential transform for invariant color image description," *Appl. Math. Comput.*, vol. 256, pp. 951–967, Apr. 2015.
[39] T. Suk and J. Flusser, "Affine moment invariants of color images," in *Proc. Int. Conf. Comput. Anal. Images Patterns*, Sep. 2009, pp. 334–341.
[40] K. M. Hosny and M. M. Darwish, "A kernel-based method for fast and accurate computation of PHT in polar coordinates," *J. Real-Time Image Process.*, vol. 16, no. 4, pp. 1235–1247, Aug. 2019.
[41] Y. Xin, M. Pawlak, and S. Liao, "Accurate computation of Zernike moments in polar coordinates," *IEEE Trans. Image Process.*, vol. 16, no. 2, pp. 581–587, Feb. 2007.
[42] C. Camacho-Bello, A. Padilla-Vivanco, C. Toxqui-Quitl, and J. J. Báez-Rojas, "Reconstruction of color biomedical images by means of quaternion generic Jacobi-Fourier moments in the framework of polar pixels," *J. Med. Imag.*, vol. 3, no. 1, Mar. 2016, Art. no. 014004.
[43] K. M. Hosny, M. M. Darwish, and T. Aboelenen, "Novel fractional-order polar harmonic transforms for gray-scale and color image analysis," *J. Franklin Inst.*, vol. 357, no. 4, pp. 2533–2560, Mar. 2020.
[44] J. D. Faires and R. L. Burden, *Numerical Methods*, 3rd ed. Pacific Grove, CA, USA: Brooks Cole Publication, 2002.
[45] Z. Hua, Y. Zhou, and H. Huang, "Cosine-transform-based chaotic system for image encryption," *Inf. Sci.*, vol. 480, pp. 403–419, Apr. 2019, doi: 10.1016/j.ins.2018.12.048.

KHALID M. HOSNY (Member, IEEE) was born Zagazig, Egypt, in 1966. He received the B.Sc., M.Sc., and Ph.D. degrees from Zagazig University, in 1988, 1994, and 2000, respectively. From 1997 to 1999, he was a Visiting Scholar with the University of Michigan, Ann Arbor, USA, and the University of Cincinnati, Cincinnati, USA. He is a Professor of Information Technology with the Faculty of Computers and Informatics, Zagazig University. He published three edited books and more than 80 articles in international journals. His research interests include image processing, pattern recognition, multimedia, and computer vision. He is an editor and scientific reviewer for more than 40 international journals. He is a Senior Member of ACM.

MOHAMED M. DARWISH received the B.Sc. (Hons.), M.Sc., and Ph.D. degrees in computer science from the Faculty of Science, Assiut University, Assiut, Egypt. He is an Assistant Professor of Computer Science with the Faculty of Computers and Information, Assiut University. His research interests include image processing, association rule mining, and medical Image analysis.

MOSTAFA M. FOUDA (Senior Member, IEEE) received the Ph.D. degree in information sciences from Tohoku University, Japan, in 2011. He has served as an Assistant Professor at Tohoku University. He has also worked as a Postdoctoral Research Associate at Tennessee Technological University, TN, USA. He is currently an Assistant Professor with Idaho State University, ID, USA. He also holds the position of Associate Professor with Benha University, Egypt. He has published over 40 articles in IEEE conference proceedings and journals. His research interests include cybersecurity, machine learning, blockchain, the IoT, 5G networks, and smart grid communications. He has served on the technical committees of several IEEE conferences. He is also a reviewer in several IEEE transactions/magazines. He is an Editor for IEEE TRANSACTIONS ON VEHICULAR TECHNOLOGY and an Associate Editor for IEEE ACCESS.